

# Nonadiabatic Quantum Dynamics Explores Non-monotonic Photodissociation Branching of N<sub>2</sub> into the N(<sup>4</sup>S)+N(<sup>2</sup>D) and N(<sup>4</sup>S)+N(<sup>2</sup>P) Product Channels

Natalia Gelfand,<sup>1\*</sup> Ksenia Komarova,<sup>1</sup> Françoise Remacle,<sup>1,2</sup> and Raphael D. Levine<sup>1,3,4</sup>

<sup>1</sup> The Fritz Haber Center for Molecular Dynamics, Institute of Chemistry, The Hebrew University of Jerusalem, Jerusalem 91904, Israel

<sup>2</sup> Theoretical Physical Chemistry, UR MolSys B6c, University of Liège, B4000 Liège, Belgium

<sup>3</sup> Department of Molecular and Medical Pharmacology, David Geffen School of Medicine and

<sup>4</sup> Department of Chemistry and Biochemistry, University of California, Los Angeles, CA 90095, USA

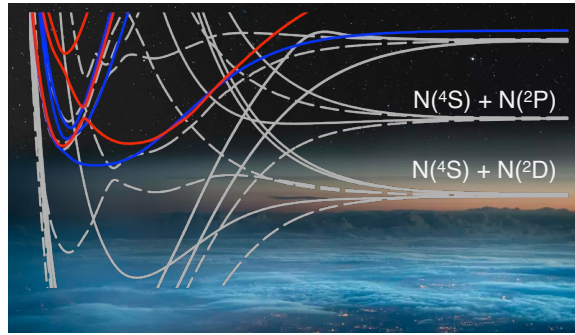
\*natalia.gelfand@mail.huji.ac.il

## ABSTRACT

Vacuum UV Photodissociation of N<sub>2</sub> molecules is a source of reactive N atoms in the interstellar medium. In the energy range of optical excitation of N<sub>2</sub>, the N-N triple bond cleavage leads to three types of atoms: ground-state N(<sup>4</sup>S) and excited-state N(<sup>2</sup>P) and N(<sup>2</sup>D). The latest is the highest reactive and it is believed to be the primary participant in reactions with hydrocarbons in Titan's atmosphere. Experimental studies have observed a non-monotonic energy dependence and non-statistical character of the photodissociation of N<sub>2</sub>. This implies different dissociation pathways and final atomic products for different wavelength regions in the sunlight spectrum. We here apply *ab initio* quantum chemical and nonadiabatic quantum dynamical techniques to follow the path of an electronic state from the excitation of a particular singlet <sup>1</sup>Σ<sub>u</sub><sup>+</sup> and <sup>1</sup>Π<sub>u</sub> vibronic level of N<sub>2</sub> to its dissociation into different atomic products. Our computations show that the strength of the spin-orbit coupling between the singlet and triplet electronic states, a resonance between the singlet and triplet eigenstates and the shape of the triplet <sup>3</sup>Π<sub>u</sub> potentials are the key components determining the efficacy of singlet to triplet population transfer and therefore predissociation lifetimes and branching ratios.

KEYWORDS: active nitrogen, branching fraction, photodissociation in the upper atmosphere, spin-orbit coupling

# TOC



## 1. Introduction

Space missions and radio astronomy can analyze the composition of upper levels of Earth's atmosphere, the atmospheres of other bodies in space and the interstellar medium. Up to nowadays, more than 200 individual molecular species from diatomic  $H_2$  and  $N_2$  to polyatomic Buckminsterfullerene and Rugbyballene were identified in space.<sup>1,2</sup> These recent discoveries have formed the basis for astrochemistry, the study of molecular structure and processes in the interstellar medium.<sup>3-5</sup>

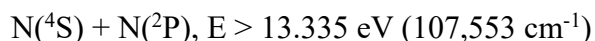
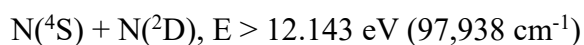
The molecules that have been identified in space are composed of 19 different elements, but carbon, hydrogen, nitrogen, and oxygen predominate. Despite the diversity of space chemistry, the main components of interstellar medium are  $H_2$  and CO and only in the atmospheres of Earth, Pluto, Titan, and Triton have significant amounts of  $N_2$  been detected. This makes  $N_2$  the most abundant nitrogen-containing molecule in the interstellar medium. However, the astrochemistry of nitrogen is diverse and rich: there are 92 different nitrogen-containing species<sup>1</sup> from diatomic CN (cyano radical)<sup>6-8</sup> and NO (nitric oxide)<sup>9,10</sup> to triatomic CaNC (calcium isocyanide)<sup>11</sup> and polyatomic  $CH_2NH$  (methanimine)<sup>12,13</sup> and  $(NH_2)_2CO$  (urea)<sup>14</sup>. This has resulted in a great interest in the chemistry of  $N_2$  in Earth's and Titan's atmospheres, where  $N_2$  molecules are the major constituent.<sup>15-19</sup> Combination of lab experiments in plasma and computer simulations shows possible reactions of the activated forms of  $N_2$  with  $CH_4$  and  $C_2H_4$  in Titan's atmosphere.<sup>20-22</sup> To understand the mechanism of these reactions and their complexity, one should have a closer look at the electronic structure of  $N_2$ .

The nitrogen molecule in its ground electronic state is a textbook example of high chemical stability: under standard conditions on Earth, its triple covalent bond is believed to be among the strongest known in nature. At the same time, nitrogen-containing molecules – purines, pyrimidines, pyrroles and indoles – play the essential role in life, and it is important to find out how the inert  $N_2$  molecule can be converted in nature into more chemically active forms. Early studies proposed a possible active nitrogen:<sup>23,24</sup>  $N_2$  in its vibrationally excited ground state  $X^1\Sigma_g^+$  and in the metastable electronically excited  $A^3\Sigma_u^+$  state or excited-state N atoms. The optically excited states of  $N_2$  are high in energy: from 12.4 to 14.8 eV relative to its ground state. Only in upper levels of Earth's atmosphere, which are not shielded by the ozone layer, the sunlight covers this energy range and nitrogen molecules can be excited and then dissociate into nitrogen atoms in their ground and excited states. The chemical reactivity of the resulting nitrogen atoms is not equal. The ground-state  $N(^4S)$  is known to be rather

inert while the excited atoms are chemically active and even further, among  $N(^2P)$  and  $N(^2D)$  the latter is known to be much more reactive.<sup>25-27</sup> Today, excited  $N(^2D)$  atoms are believed to play the principal role in reactions with  $H_2$  and hydrocarbons and forming HCN,  $C_2N_2$  and other compounds in low-pressure space environments.<sup>28-31</sup>

The first step in generation of chemically active nitrogen atoms from is the optical excitation of the molecule in the VUV spectral region. The absorption spectrum of  $N_2$  from 100,000 to 120,000  $cm^{-1}$  was extensively studied both experimentally<sup>32,33</sup> and theoretically.<sup>34</sup> Following classification based on selection rules, two types of one-photon optically accessible singlet states are possible for excitation from the electronic ground state:  $^1\Sigma_u^+$  and  $^1\Pi_u$ . These states are reached by a parallel or perpendicular orientation of the molecule relative to the light field and these states of different symmetry do not interact with one another. However, states of the same symmetry and multiplicity can be coupled by nonadiabatic terms and so the electronic states of either  $^1\Sigma_u^+$  or  $^1\Pi_u$  symmetry can be mixed among themselves. In the extensively studied lower energy range these states are bound.

The way to dissociation is through spin-orbit induced transfer from the singlets to the states of higher multiplicity which are dissociative. The photodissociation of  $N_2$  has been experimentally studied by, first, electron impact<sup>35</sup> and further with fast-beams<sup>36-38</sup> and wavelength selected VUV excitation.<sup>39,40</sup> The latter was with special reference to isotopic selectivity. The most recent detailed work uses supersonic molecular beams coupled with velocity-mapped imaging method.<sup>41-44</sup> In the energy range up to 120,000  $cm^{-1}$ , there are three dissociation limits which lead to excited-state N atoms in the following states at the given thresholds:



The experiments consistently exhibit strong energy dependence in the photodissociation branching fractions: different predissociative  $N_2$  states with similar internal energies are found to follow different dissociation pathways, thereby suggesting that the unimolecular dissociation is not statistical.

Experimental studies provide the accurate information on the final dissociation products but do not explain the origin of their energy dependence. Here theoretical approaches can be essential. High-level *ab initio* quantum chemistry methods allow a close examination of a

group of electronic states of comparable energies so that one can simulate a realistic dependence of the potential energy of different electronic states on changes in the molecular bond distance. Quantum chemical calculations have accompanied experiments in interpretation of the electronic structure of N<sub>2</sub> in many directions: vibronic states energies and composition,<sup>45,46</sup> nature of electronic transitions<sup>47,48</sup> and band complexes.<sup>49,50</sup> The potential energy curves were studied in detail<sup>51–58</sup> as well as the spin-orbit<sup>55</sup> and nonadiabatic couplings.<sup>59</sup> Nowadays the quantum dynamical approaches<sup>60–63</sup> have reached a level where they can offer a computational tool which allowed us to follow the time-evolution of an electronic wave packet travelling in the forest of electronic states, beyond the states directly accessed from the ground electronic state.<sup>64</sup>

We recently computationally simulated a realistic energy dependence in the dissociation branching arising from excitation of different single vibrational levels of  $^1\Sigma_u^+$  electronic states of N<sub>2</sub>. These computations started from the molecule in the ground electronic states and excited it by a polarized laser pulse of a very long duration and of the required mean energy. In the present work we make a step further and present the results of the branching into the channels N(<sup>4</sup>S) + N(<sup>2</sup>D) (Channel 1) and N(<sup>4</sup>S) + N(<sup>2</sup>P) (Channel 2) accessed through the excited  $^1\Pi_u$  states of N<sub>2</sub>. We highlight the differences in the results for these two distinct doorway excited states. First, following excitation of  $^1\Sigma_u^+$  states there is an early opening of Channel 2 at 110,000 which is absent for  $^1\Pi_u$ . Also, from 112,000 to 115,000 cm<sup>-1</sup> there are oscillating changes in branching for  $^1\Pi_u$  while for  $^1\Sigma_u^+$  the change is smooth. For both types of the singlets, a drop is present at 115,000 cm<sup>-1</sup>, but then for excited  $^1\Sigma_u^+$  there is a preferable branching fraction into Channel 2 while for  $^1\Pi_u$  the preference is for dissociation into Channel 1.

The manuscript is organized as follows: first, we review the selection rules relevant to the one-photon excitation and dissociation of N<sub>2</sub> and the computational scheme that we use for the simulations; second, we compare the dissociation branching starting from excited  $^1\Sigma_u^+$  or  $^1\Pi_u$  states; third, we discuss the predissociation lifetime and isotope effect on the dynamics and branching. We conclude with a prospective outlook on excited state dissociative dynamics in the N<sub>2</sub> molecule in connection with reaction dynamics in the upper atmosphere and in the interstellar medium.



## 2. Computational overview

### 2.1. Selection rules relevant for the one-photon excitation of $N_2$

The  $^{14}N_2$  molecule belongs to  $D_{\infty h}$  point group. This means the presence of inversion through a center of symmetry and infinite number of horizontal mirror planes intersecting the principal symmetry  $Z$  axis along the N-N bond. Therefore, all the electronic states can be classified either “gerade” or “ungerade” relative to the inversion operation. In the present paper, we discuss one photon VUV excitation of  $N_2$  from its ground state  $X^1\Sigma_g^+$ . The dipole allowed transitions are those with the change of parity and so only  $^1\Sigma_u^+$  and  $^1\Pi_u$  can be optically accessed. The symmetry of the final state depends on the orientation of the molecule relative to the laser: if the molecule aligns along X/Y axis,  $^1\Pi_u$  states will be reached and if it aligns along  $Z$  axis –  $^1\Sigma_u^+$  states. These singlet states are coupled to other “ungerade” states of higher multiplicity via spin-orbit coupling.

There are three Cartesian components of the spin-orbit coupling integrals that differ along X, Y and Z axes in the molecular frame. According to their orbital momentum  $\Lambda$ , all the states can be labeled as  $\Sigma, \Pi, \Delta$  etc. Triplet and quintet electronic states are degenerate states with different  $S_z$  projection ( $m_S = -1, 0, 1$  for triplets and  $m_S = -2, -1, 0, 1, 2$  for quintets). The selection rules of the spin-orbit coupling play a key role in the interconnections of manifolds of states of different multiplicities. Two states with  $\Delta\Lambda = 0$  are coupled by the  $Z$  component of the spin orbit coupling, that we denote as LSZ and these two interacting states must have the same magnetic quantum number,  $\Delta m_S = 0$ . Two states with  $\Delta\Lambda = \pm 1$  are coupled by the LSX/LSY component of the coupling and must differ as  $\Delta m_S = \pm 1$ . The implication is that while both singlet  $^1\Sigma_u^+$  and  $^1\Pi_u$  electronic states can interact with the triplets the triplet states that they couple to are different.  $^1\Sigma_u^+$  singlet states are coupled by LSX/LSY component of the spin-orbit interaction to the  $^3\Pi_u$  states and only  $m_S = \pm 1$  of the triplet states can be populated.  $^1\Pi_u$  are coupled by LSZ spin-orbit interaction to the  $^3\Pi_u$  states and for this type of coupling the selection rule is  $\Delta m_S = 0$ . Similar considerations apply to coupling to the quintets: LSZ spin-orbit interaction between  $^3\Pi_u$  and  $^5\Pi_u$  and LSX/LSY

spin-orbit coupling between  $^3\Pi_u$  and  $^5\Sigma_u^+$ . Therefore, a particular singlet state of  $^1\Sigma_u^+$  or  $^1\Pi_u$  symmetry can lead to a different manner of exit to the dissociative channels

The states of the same symmetry and multiplicity are coupled by nonadiabatic interaction, and they can exchange population among themselves in the avoided crossings regions. We have included the nonadiabatic coupling among  $^1\Sigma_u^+$ ,  $^1\Pi_u$ ,  $^3\Pi_u$  states. More details on selection rules can be found in <sup>65</sup>.

## 2.2. Quantum chemical calculations

We consider the states in energy range 90,000 – 120,000  $\text{cm}^{-1}$  where the dissociation channels 1 and 2 are open, see Figure 1. Thus, the electronic basis we use consist of the ground  $X^1\Sigma_g^+$  state and the following excited electronic states: three  $^1\Sigma_u^+$ , three  $^1\Pi_u$ , one  $^1\Sigma_u^-$ , one  $^1\Delta_u$ , one  $^3\Sigma_u^+$ , one  $^3\Sigma_u^-$ , four  $^3\Pi_u$ , one  $^3\Delta_u$ , one  $^5\Sigma_u^+$ , one  $^5\Sigma_u^-$ , two  $^5\Pi_u$  and one  $^5\Delta_u$ . 21 electronic states in all, and accounting for their magnetic degeneracy a total of 55 quantum electronic states.

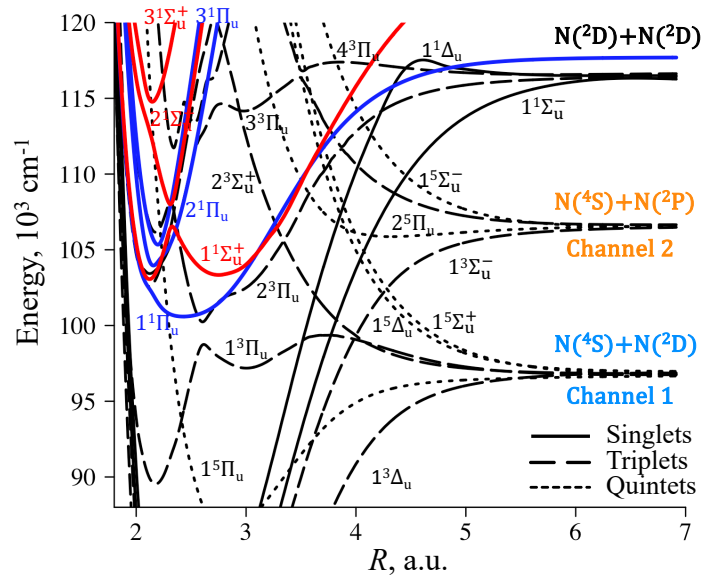


Figure 1. Potential energy curves of “ungerade” electronic states of the nitrogen molecule in energy range 90,000 – 120,000  $\text{cm}^{-1}$ . The singlets are the states that can be optically accessible by one photon from the “gerade” ground electronic state.  $^1\Sigma_u^+$  singlet states are

shown in red and  $^1\Pi_u$  are in blue. Other singlet states are shown with solid black lines, the triplet states with dashed lines and quintets with dotted lines. The lowest dissociative channels are in blue and orange.

The terms of the electronic Hamiltonian (electronic potential energy curves, non-adiabatic and spin-orbit couplings) of  $N_2$  in the VUV energy range are calculated for each value of internuclear distance using a state-averaged complete active space self-consistent field (CASSCF) approach followed by multi-reference configuration interaction (MRCI)<sup>66,67</sup> calculations. An active space of 17 orbitals ( $4\sigma_u$ ,  $3\sigma_g$ ,  $4\pi_u$ ,  $4\pi_g$ , and  $2\delta_g$ ) for 10 valence electrons was employed in all computations. The two lowest  $1\sigma_u$  and  $1\sigma_g$  orbitals were not included in the active space but are fully optimized in the CASSCF procedure. Restriction of only single occupancy for the higher Rydberg orbitals was used. We chose a doubly augmented cc-pVQZ basis set with additional bond-centered s and p diffuse functions for a proper description of Rydberg and valence singlet and triplet states according to the previously established methodology.<sup>34</sup> All the quantum chemistry calculations are performed with the MOLPRO program package.<sup>68,69</sup> The computed potential energy curves were shifted by  $850\text{ cm}^{-1}$  to be in accordance with previously published data.<sup>34</sup>

The potential energy curves, nonadiabatic coupling and dipole moments of  $^1\Pi_u$  states were taken in analytical form from <sup>34</sup> and adiabaticized as explained in <sup>64</sup>. The derived adiabatic data along with presently computed spin-orbit coupling elements are given in Figures S1-S7 of the Supporting Information (SI).

### 2.3. *Nonadiabatic quantum dynamics*

We use the time-dependent Schrodinger equation of motion to compute quantum dynamics on a grid of internuclear distance for the 54 excited and 1 ground electronic states of definite multiplicity. The equation of motion is defined for the amplitudes  $C_{ng} = \Psi_n(R_g)$  at a given electronic state  $n$  and grid point  $g$  for the internuclear distance  $R = R_g$ , see <sup>70</sup>, are the solutions of equation (1):

$$\begin{aligned}
i\hbar \frac{dC_{ng}}{dt} = & (T^d + V_n(R_g))C_{ng} - iV_{CAP}(R_g)C_{ng} + \sum_{q=1}^2 T_q^{off} (C_{n,g+q} + C_{n,g-q}) \\
& - \sum_{k=1}^{N_e} \sum_{q=1}^2 p_q \left( (\tau_{nk}(R_g) + \tau_{nk}(R_{g-q}))C_{k,g-q} - (\tau_{nk}(R_g) + \tau_{nk}(R_{g+q}))C_{k,g+q} \right) \\
& - \sum_{k=1}^{N_e} \left( E(t)\mu_{nk}(R_g) + \frac{1}{2m} \sum_{l=1}^{N_e} \tau_{nl}(R_g) \cdot \tau_{lk}(R_g) - H_{nk}^{SO}(R_g) \right) C_{kg}
\end{aligned} \quad (1)$$

Here  $T^d$  and  $T_q^{off}$  are diagonal and off-diagonal kinetic energy terms, respectively, evaluated using a five-point finite difference approximation, see Ref. 70  $V_n(R)$  denotes potential energy of an electronic state  $n$ . At large internuclear distances,  $R > 6.2$  a.u., a complex absorbing potential,  $V_{CAP}(R) = 0.01 \cdot (R - 6.2)^3$ , is applied for all the dissociative states. The non-adiabatic couplings  $\tau_{nk}(R)$  between electronic states  $n$  and  $k$  are scaled by the finite difference momentum terms,  $p_q$ . The propagation of the equation **Error! Reference source not found.** is solved via the Runge-Kutta method with a time step of  $\Delta t = 10^{-4}$  fs and  $\Delta R = 0.005$  a.u. for the grid spacing. The propagation lasted for 5 ps in all the dynamical calculations. The lifetimes of the excited vibrational singlet states are estimated by a linear fit for the logarithm of their time-dependent population,  $|C_{ng}(t)|^2$ , assuming a unimolecular exponential decay.

The interaction with the light field is governed by the transition dipole moment  $\mu_{nk}(R)$  between the ground  $X^1\Sigma_g^+$  and excited singlet electronic states. An explicit time-profile for the VUV light field is used with a very long duration

$$E(t) = \boldsymbol{\varepsilon}_p \cdot E_{\max} \cdot \exp\left(-\frac{(t-t_p)^2}{2\sigma_p^2}\right) \left[ \cos(\omega_p t) - \left(\frac{t-t_p}{\omega_p \sigma_p^2}\right) \sin(\omega_p t) \right] \quad (2)$$

Here  $\boldsymbol{\varepsilon}_p$  is the polarization direction of the light field, set along the internuclear axis so as to access the  $^1\Sigma_u^+$  states and perpendicular to the internuclear axis to reach the  $^1\Pi_u$  states.  $E_{\max}$  is the maximum amplitude of the field;  $t_p$  and  $\sigma_p$  are the time at which the pulse is centered and the width of the Gaussian envelope of the field.

Duration of the pulse was set to be long enough to selectively excite specific vibrational levels of the singlet states,  $\sigma_p = 160$  fs,  $t_p = 1,200$  fs and  $E_{\max} = 0.0001$  au. The carrier

frequency  $\omega_p$  was varied from 108,000 to 116,000  $\text{cm}^{-1}$  according to the energy of the vibrational levels obtained by diagonalization in the singlets manifold. The choice of this energy range was determined by the thresholds of two dissociation channels.

Given all the above information, the Hamiltonian can be represented as a sparse square matrix, as shown in Figure 2. The potential energies of the electronic states form diagonal elements, and the various coupling terms are off-diagonal ones. These terms can link states of the same symmetry and multiplicity (non-adiabatic or spin-orbit couplings, shown in light-red, light-green, and light-blue) or states of different multiplicity (yellow and cyan off-diagonal blocks).

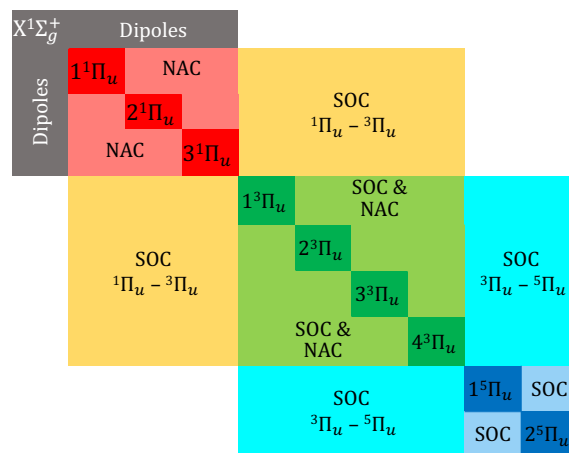


Figure 2. A schematic representation of the Hamiltonian which includes the ground electronic state  $X^1\Sigma_g^+$ , singlet  $1^1\Pi_u$ , triplet  $3^3\Pi_u$  and quintet  $5^5\Pi_u$ . The singlet  $1^1\Pi_u$  states are coupled by X/Y components of the transition dipole moments with the ground state  $X^1\Sigma_g^+$  (the dark-grey block). In the calculations, such a block is comprised by more excited states, and it is formed for each internuclear N-N grid point from 1.0 to 7.5 a.u. with the grid spacing of 0.005 a.u., 1301 blocks in total for each time point along 5 ps propagation. The same structure of Hamiltonian is applied to the singlet  $1^1\Sigma_u^+$  states which are coupled by Z components of the transition dipole moments with the ground state  $X^1\Sigma_g^+$ .

### 3. Results and Discussion

#### 3.1. *Optically excited and dissociative states of N<sub>2</sub>*

The N<sub>2</sub> molecule dissociates indirectly and the excited  $^1\Sigma_u^+$  and  $^1\Pi_u$  singlets are the (rather narrow) doorways in the population transfer from the ground  $X^1\Sigma_g^+$  state to the dissociative electronic states.<sup>71</sup> For both types of the singlets, there are two bound (Rydberg) and one delocalized (valence) states. However, the  $^1\Pi_u$  states all are lower-lying and are more strongly mixed by nonadiabatic interaction in the energy range of 100,000 – 107,000 cm<sup>-1</sup> while the  $^1\Sigma_u^+$  states are more energetically separated from one another and from  $2^3\Pi_u$  and  $3^3\Pi_u$  state, see Figure 3(a).

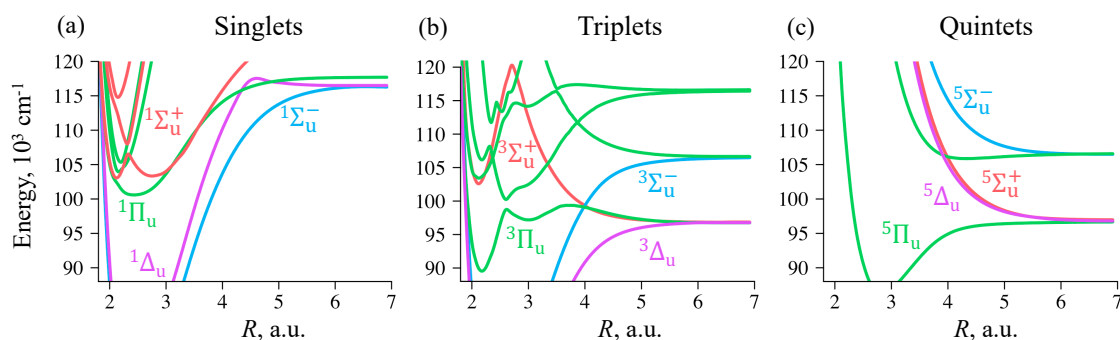


Figure 3. Potential energy curves of singlet (a), triplet (b) and quintet (c) multiplicity color-coded according to the symmetry of the states:  $^1\Sigma_u^+$ ,  $^3\Sigma_u^+$  and  $^5\Sigma_u^+$  are in orange-red,  $^1\Sigma_u^-$ ,  $^3\Sigma_u^-$ ,  $^5\Sigma_u^-$  are in light-blue;  $^1\Pi_u$ ,  $^3\Pi_u$ ,  $^5\Pi_u$  are in mint green;  $^1\Delta_u$ ,  $^3\Delta_u$ ,  $^5\Delta_u$  are in magenta.

The  $^3\Pi_u$  triplets are believed to be the main doorway to the single photon VUV dissociation of the N<sub>2</sub> molecule. Three distinct dissociation channels can be seen in the energy range from 90,000 to 120,000 cm<sup>-1</sup> and two lower ones are labeled as “Channel 1” and “Channel 2” in Figure 1. The triplet states are composed of bound parts when the internuclear distance,  $R$ , is shorter than 2.7 au, the repulsive one from  $R > 3.5$  au and dissociative ones,  $R > 6$ . Among the other triplets,  $2^3\Sigma_u^+$  also has a distinctive structure: in the short-range distances, it is very close to  $^1\Pi_u$  and mirrors its shape. The other triplets and quintet states are primarily repulsive: there are no avoided crossings or other distinctions in their manifold.

The link between the excited states of different multiplicity is the spin-orbit coupling and the shape of the potentials predominantly affects the magnitude and sign of the spin-orbit induced transfer from the singlet to the triplet states. Figure 4 shows the results of quantum chemical calculations for the spin-orbit coupling terms between  $^1\Sigma_u^+$  and  $^3\Pi_u$  (panels a and c) and  $^1\Pi_u$  and  $^3\Pi_u$  states (panels b and d). All three lowest  $^1\Pi_u$  adiabatic states are stronger connected to the  $^3\Pi_u$  states: the coupling of 42  $\text{cm}^{-1}$  against of 30  $\text{cm}^{-1}$  in the case of  $^1\Sigma_u^+ - ^3\Pi_u$ . The delocalized  $^1\Pi_u$  state exits to the Channel 3 and so coupled to  $^3\Pi_u$  even in the region of its avoiding crossing at 4 a.u.

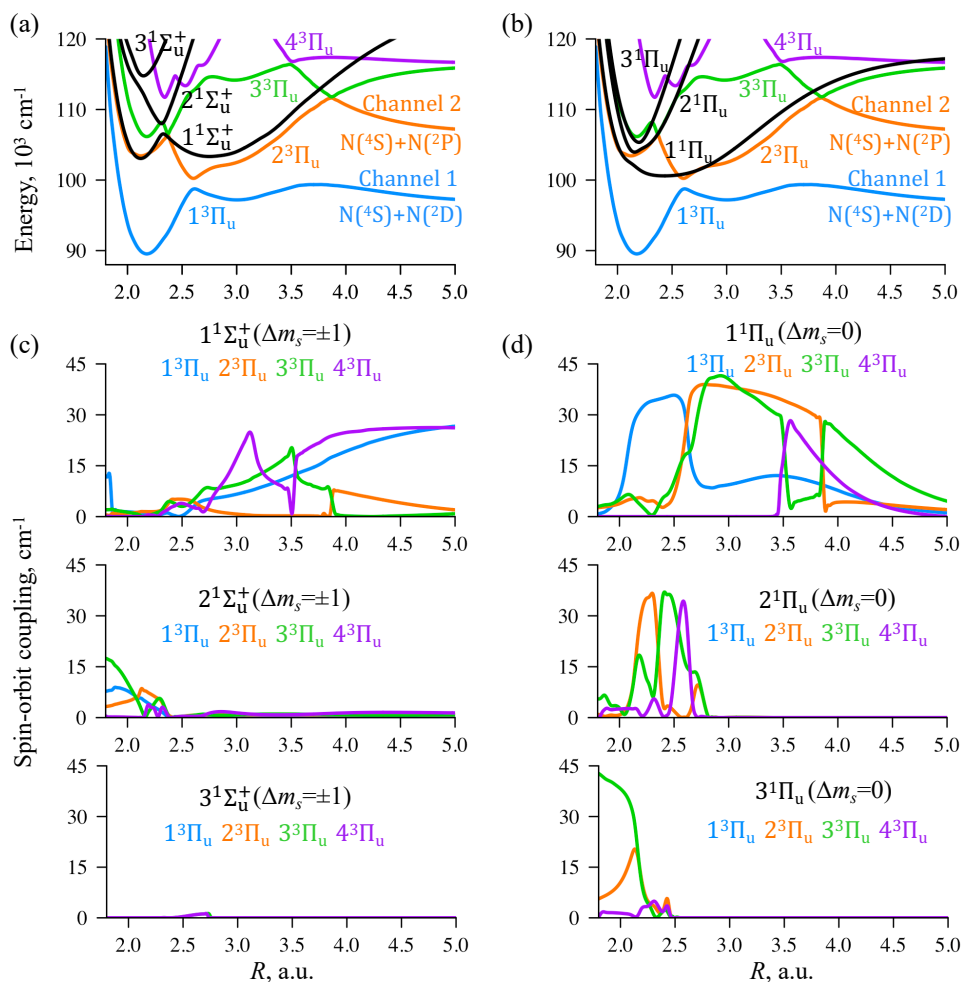


Figure 4. (a) Potential energy curves of  $^1\Sigma_u^+$  (in black) and  $^3\Pi_u$  (color-coded in the figure) and the absolute values of the spin-orbit coupling terms between them; (b)  $^1\Pi_u$  and (in black) and  $^3\Pi_u$  (color-coded in the figure) and the spin-orbit coupling terms between them.

The singlets are also coupled to other triplet states:  ${}^1\Sigma_u^+$  can interact with  ${}^3\Sigma_u^-$  while  ${}^1\Pi_u$  interacts with  ${}^3\Sigma_u^+$ ,  ${}^3\Sigma_u^-$  and  ${}^3\Delta_u$ . However, our computations give rather small couplings among the states mentioned above and the largest is of  $12\text{ cm}^{-1}$  between  ${}^1\Pi_u$  and  $2{}^3\Sigma_u^+$  states, see Figures S4-S7 of the SI.

### 3.2. Energy dependence in photodissociation branching fractions

The non-statistical character of the dissociation of  $\text{N}_2$  was noted already in 1988 by Helm and Cosby<sup>36</sup> and the experiment of Song *et al*<sup>41</sup> confirmed a non-monotonic energy dependence in the dissociation branching fractions. These experimental works suggested the presence of various pathways to dissociation determined by the initial excited vibronic level of the singlet states. The experimental results for  ${}^1\Sigma_u^+$  and  ${}^1\Pi_u$  states are significantly different (black lines in Figure 5):

(1) in the case of  ${}^1\Sigma_u^+$ , there is an early opening of Channel 2 at  $110,000$  which is absent for  ${}^1\Pi_u$ ;

(2) above the avoiding crossing between  $2{}^3\Pi_u$  and  $3{}^3\Pi_u$  where the triplet repulsive potential is available (from  $112,000$  to  $115,000\text{ cm}^{-1}$ ) there are oscillating changes in branching for  ${}^1\Pi_u$  and a smooth change for  ${}^1\Sigma_u^+$ ;

(3) in both cases, a drop is present at  $115,000\text{ cm}^{-1}$ , but then for excited  ${}^1\Sigma_u^+$  there is a preferable branching fraction into Channel 2 while for  ${}^1\Pi_u$  the branching is favored into Channel 1.

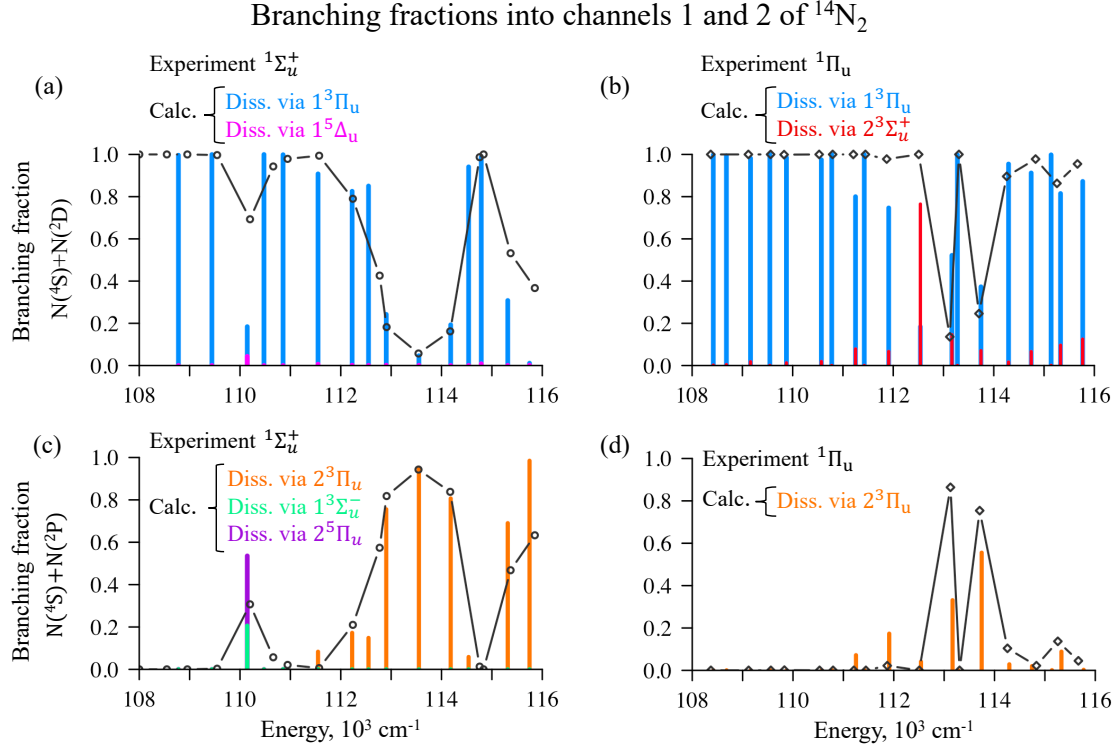


Figure 5. Experimental (black line) and calculated (histograms color-coded in the figure) branching fractions in Channel 1 (panels a and b) and in Channel 2 (panels c and d) obtained by exciting vibronic levels of  $^1\Sigma_u^+$  (panels a and c) or  $^1\Pi_u$  (panels b and d) states of the  $^{14}\text{N}_2$  molecule.

To investigate an intricate pathway of electronic subsystem on its way from excitation of a particular vibronic level of singlets to dissociation, we performed quantum dynamical calculations on a grid of the N-N internuclear coordinate. These calculations are based on the results of *ab initio* quantum chemical computations at CASSCF/MRCI level. The states of triplet and quintet multiplicity of *u* parity from 90,000 to 120,000  $\text{cm}^{-1}$  were included in the Hamiltonian, more details are given in section 2.

Figure 5 shows the computed branching fractions into Channel 1 and Channel 2 versus the experimental data. The calculations have captured several key features of the experiment and therefore allow us to deliver a detailed explanation on the questions pointed above. First of all, one can see the major contribution of  $^3\Pi_u$  states to the dissociation:  $1^3\Sigma_u^-$ ,  $1^3\Delta_u$  and  $2^5\Pi_u$  contribute at 110,000  $\text{cm}^{-1}$  only.  $2^3\Sigma_u^+$  plays a major role due to a higher spin-orbit coupling with  $^1\Pi_u$ .

Figure 6 presents the snapshots of the dynamics. Let us first highlight the similarity between the branching starting from the two singlets. The principal one is the dissociation into Channel 2 at 113,000  $\text{cm}^{-1}$ : the repulsive triplet  $^3\Pi_u$  is accessible here for both singlets and the prompt dissociation occurs (Figure 6b and 6f). At other lower energies, Channel 1 is almost always preferable and also at 115,000  $\text{cm}^{-1}$  when the triplet is trapped.

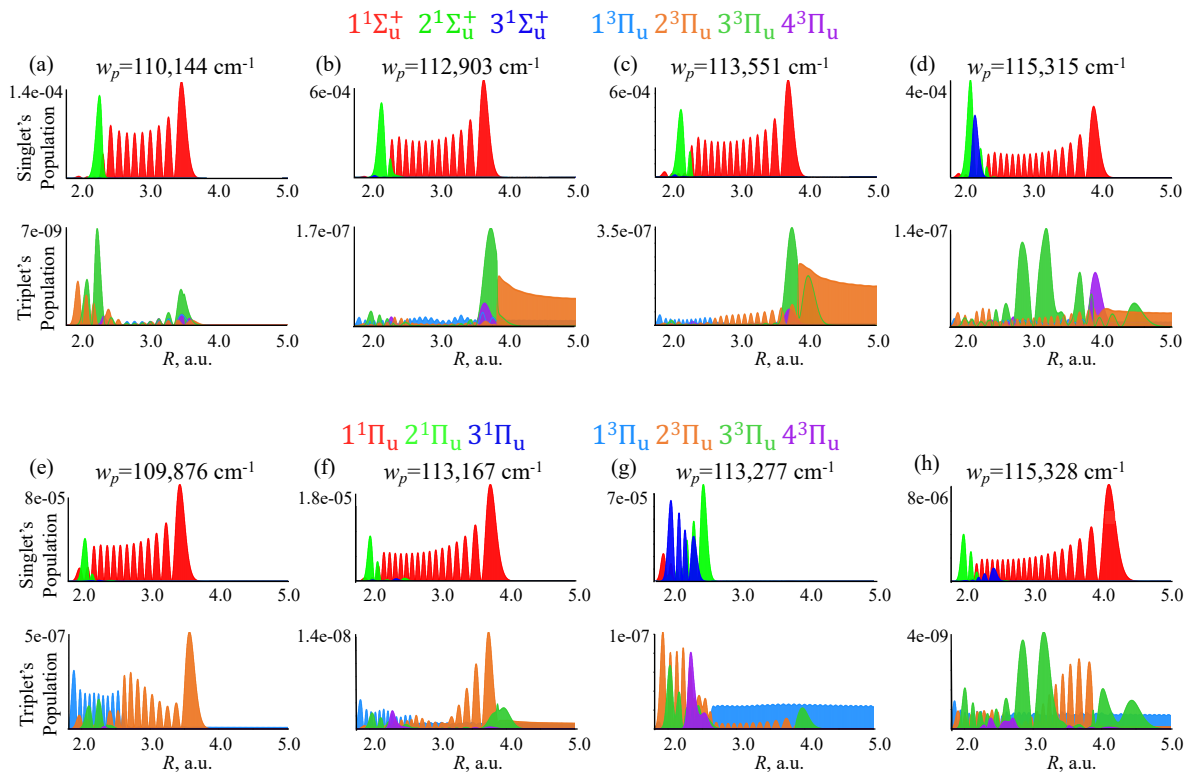


Figure 6. Population redistribution in the singlet and triplet manifolds at 5 ps obtained by exciting vibronic levels of  $^1\Sigma_u^+$  (panels ) or  $^1\Pi_u$  (panels ) states of the  $^{14}\text{N}_2$  molecule. The three selected energies show a similar trend for both types of the singlets. The three selected energies show major differences for the two types of the singlets.

There are clear differences between the two singlet sites. Under excitation of  $^1\Sigma_u^+$  at 110,144  $\text{cm}^{-1}$ , Channel 2 opens. As one can see in Figure 6a, the population of the triplets  $^3\Pi_u$  is very low and so even other low populated states become important. The next difference is a rapid change at 113,277  $\text{cm}^{-1}$  for  $^1\Pi_u$ . Figure 6g shows the singlet vibronic state of the Rydberg character and because of strong spin-orbit interaction between  $^1\Pi_u$  and  $^3\Pi_u$ , this Rydberg singlet state is effectively populating the bound triplet. The third

difference is at  $115,300 \text{ cm}^{-1}$  where  $1\Sigma_u^+$  occurs to be in resonance with the repulsive  $3\Pi_u$  potential while  $1\Pi_u$  is attached to the bound  $3\Pi_u$ . However, both singlets contribute to Channel 2 at  $113,000 \text{ cm}^{-1}$  which is just above the avoiding crossing between  $2^3\Pi_u$  and  $3^3\Pi_u$  states.

### 3.3. Predissociation lifetime and isotope effect in photodissociation branching fractions

The recent experiment of <sup>42</sup> showed the mass effect in the branching, which is primarily seen in the fraction of the products exiting in Channel 2. The results of the computations along with the experimental results are depicted for the isotopomer  $^{14}\text{N}^{15}\text{N}$  in Figure 7. While the main branching fraction changes are the same for  $^{14}\text{N}_2$  and  $^{14}\text{N}^{15}\text{N}$ , the theory predicts a significant change in contributing of  $2^3\Sigma_u^+$  states into Channel 2: even the small mass difference influence the resonance between the singlet and triplet states and makes the transfer easier.

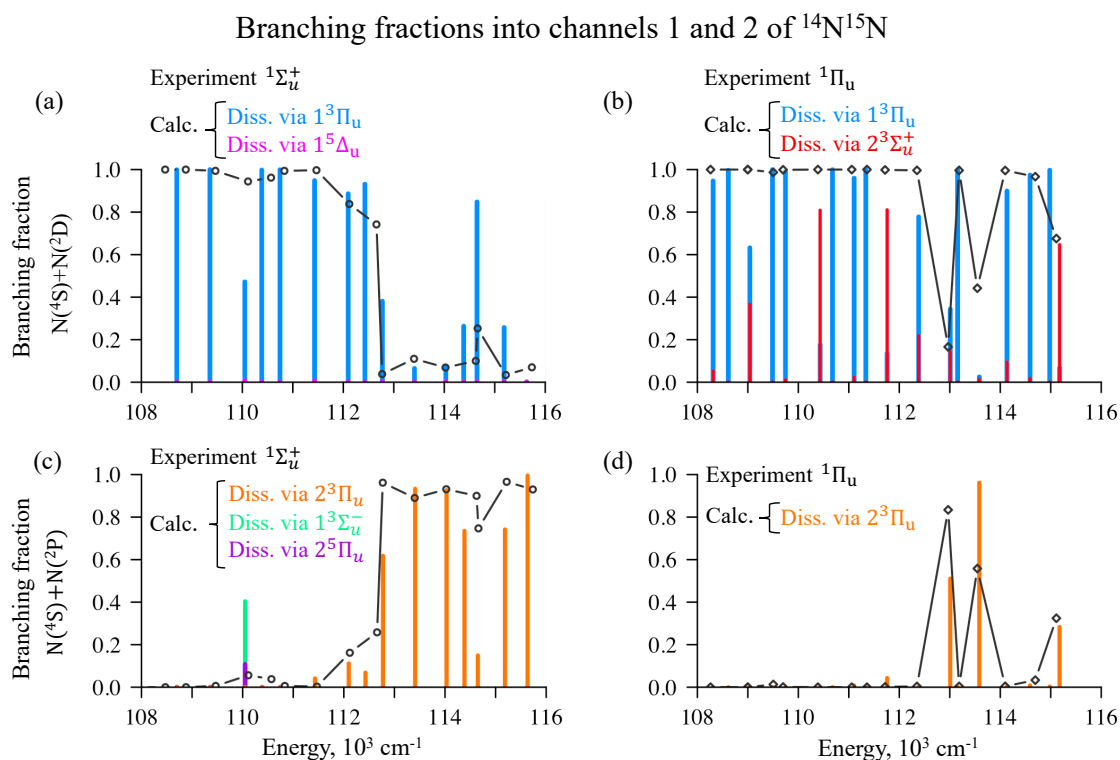


Figure 7. Experimental (black line with circles) and calculated (histograms are color-coded in the figure) branching fractions in Channel 1 (panels a and b) and in Channel 2 (panels c and d) obtained by exciting vibronic levels of  $1\Sigma_u^+$  (panels a and c) or  $1\Pi_u$  (panels b and d) states of the  $^{14}\text{N}^{15}\text{N}$  molecule.

Another characteristic of the photodissociation is the predissociation singlet lifetime which indicate the how fast or slow the initial wave packet will be transferring from the excited singlet state to the dissociation product channel via the triplets. Figure 8 presents the calculated lifetimes for both  $^1\Sigma_u^+$  (Figure 8a) and  $^1\Pi_u$  (Figure 8b) of the two isotopomers. A key result is that the Y-axis is ten-times larger for  $^1\Sigma_u^+$ : because of a weaker coupling, these states dissociate much more slowly. In particular at the specific energy of 110,144  $\text{cm}^{-1}$  the singlets will take much longer to decay.

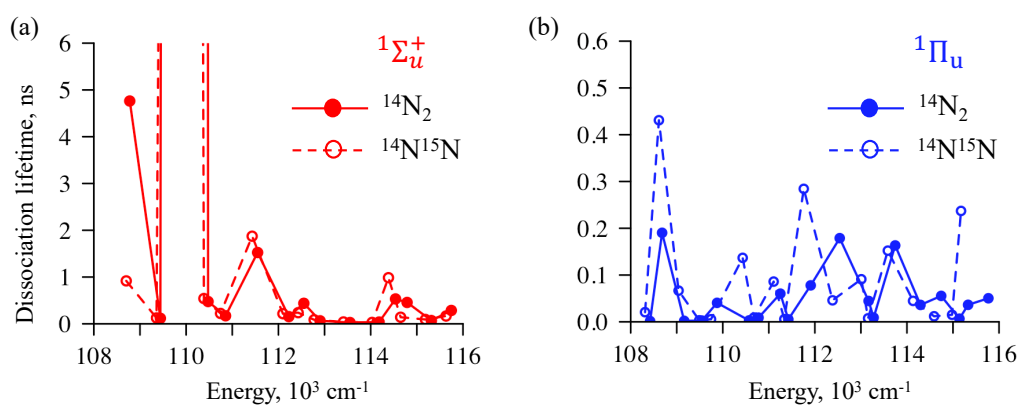


Figure 8. Calculated predissociation lifetimes obtained by exciting vibronic levels of  $^1\Sigma_u^+$  (panels a and c) or  $^1\Pi_u$  (panels b and d) states of the  $^{14}\text{N}_2$  (panels a and b) or  $^{14}\text{N}^{15}\text{N}$  (panels c and d) molecule.

#### 4. Concluding remarks

Photodissociation is the most direct way to obtain a chemically reactive nitrogen, however, the atomic composition of dissociation products cannot be easily predicted if more than one product channel is available. Combining the results of accurate experiments and state-of-art computer modelling, a better understanding of energy-dependence in the dissociation of  $N_2$  and its fractionation mechanism has been achieved. Our simulations show that the character of singlets, valence or Rydberg, and the strength of their spin-orbit coupling to the triplets determine the efficiency of population transfer and therefore predissociation lifetime. As a result of stronger coupling, excited  $^1\Pi_u$  states dissociate much faster than  $^1\Sigma_u^+$ . However, we also found the repulsive shape of the triplet  $^3\Pi_u$  potentials is in control of the prompt dissociation from 112,000 to 115,000  $cm^{-1}$ . For some energies, contribution of other states –  $2^3\Sigma_u^+$ ,  $1^3\Sigma_u^-$ ,  $2^5\Pi_u$  – have been found significant.

Therefore, the route to producing reactive  $N(^2D)$  is not straight forward and the fraction will be especially low when it is the vibronic levels of  $^1\Sigma_u^+$  that are excited. The somewhat lower in energy vibronic states of  $^1\Pi_u$  symmetry are on the contrary better coupled to the bound  $^3\Pi_u$  triplets and dissociative  $2^3\Sigma_u^+$  which allows  $N(^2D)$  to be the more favourable product. Shielding of the VUV light in the upper atmosphere can therefore play a major role in the preferential formation of the reactive  $N(^2D)$  atoms.

#### Acknowledgments

The authors acknowledge financial support of the US–Israel grant No. 2019722 NSF–BSF Astronomy and Astrophysics. F.R. acknowledges the support of the Fonds National de la Recherche (F.R.S.-FNRS, Belgium), #T0205.20.

#### References

- (1) McGuire, B. A. 2021 Census of Interstellar, Circumstellar, Extragalactic, Protoplanetary Disk, and Exoplanetary Molecules. *Astrophys. J. Suppl. Ser.* **2022**, 259 (2), 30. <https://doi.org/10.3847/1538-4365/ac2a48>.
- (2) Cami, J.; Bernard-Salas, J.; Peeters, E.; Malek, S. E. Detection of C60 and C70 in a Young Planetary Planetary Nebula. *Science (80-. )*. **2010**, 329 (1), 1180–1182.
- (3) Williams, D. A.; Cecchi-Pestellini, C. What Is Astrochemistry? In *Astrochemistry*:

- Chemistry in Interstellar and Circumstellar Space*; Royal Society of Chemistry, 2023; p 248. <https://doi.org/10.1039/9781839163968-00001>.
- (4) Bergin, E. A.; Langer, W. D.; Goldsmith, P. F. Gas-Phase Chemistry in Dense Interstellar Clouds Including Grain Surface Molecular Depletion and Desorption. *Astrophys. J.* **1995**, *441*, 222–243.
  - (5) Gonzalez, C.; Schlegel, H. B. Atmospheric Chemistry of Titan: Ab Initio Study of the Reaction between Nitrogen Atoms and Methyl Radicals. *J. AmS. Chem. Soc.* **1992**, *114* (23), 9118–9122. <https://doi.org/10.1021/ja00049a052>.
  - (6) McKellar, A. Evidence for the Molecular Origin of Some Hitherto Unidentified Interstellar Lines. *Astron. Soc. Pacific* **1940**, *52*, 187–192.
  - (7) Adams, W. S. Some Results with the COUDÉ Spectrograph of the Mount Wilson Observatory. *Astrophys. J.* **1941**, *93* (638), 11. <https://doi.org/10.1086/144237>.
  - (8) Jefferts, K. B.; Penzias, A. A.; Wilson, R. W. Observation of the CN Radical in the Orion Nebula and W51. *Astrophys. J.* **1970**, *161*, 87–89.
  - (9) Gallagher, J. J.; Johnson, C. M. Uncoupling Effects in the Microwave Spectrum of Nitric Oxide. *Phys. Rev.* **1956**, *103*, 1727–1737.
  - (10) Liszt, H. S.; Turner, B. E. Microwave Detection of Interstellar NO. *Astrophys. J.* **1978**, *224*, 73–76.
  - (11) Cernicharo, J.; Velilla-Prieto, L.; Agúndez, M.; Pardo, J. R.; Fonfría, J. P.; Quintana-Lacaci, G.; Cabezas, C.; Bermúdez, C.; Guélin, M. Discovery of the First Ca-Bearing Molecule in Space: CaNC. *Astron. Astrophys.* **2019**, *627*, L4. <https://doi.org/10.1051/0004-6361/201936040>.
  - (12) Johnson, D. R.; Lovas, F. J. Microwave Detection of the Molecular Transient Methyleneimine (CH<sub>2</sub>=NH). *Chem. Phys. Lett.* **1972**, *15*, 65–68.
  - (13) Godfrey, P. D.; Brown, R. D.; Robinson, B. J.; M.W., S. Discovery of Interstellar Methanimine (Formaldimine). *Astrophys. Lett.* **1973**, *13*, 119–121.
  - (14) Belloche, A.; Garrod, R. T.; Müller, H. S. P.; Menten, K. M.; Medvedev, I.; Thomas, J.; Kisiel, Z. Re-Exploring Molecular Complexity with ALMA (ReMoCA): Interstellar Detection of Urea. *Astron. Astrophys.* **2019**, *628*, A10. <https://doi.org/10.1051/0004-6361/201935428>.
  - (15) Vuitton, V.; Yelle, R. V.; Anicich, V. G. The Nitrogen Chemistry of Titan’s Upper Atmosphere Revealed. *Astrophys. J.* **2006**, *647* (August), 175–178.
  - (16) He, C.; Smith, M. A. Identification of Nitrogenous Organic Species in Titan Aerosols Analogs: Nitrogen Fixation Routes in Early Atmospheres. *Icarus* **2013**, *226* (1), 33–

40. <https://doi.org/10.1016/j.icarus.2013.05.013>.
- (17) He, C.; Smith, M. A. Identification of Nitrogenous Organic Species in Titan Aerosols Analogs: Implication for Prebiotic Chemistry on Titan and Early Earth. *Icarus* **2014**, *238*, 86–92. <https://doi.org/10.1016/j.icarus.2014.05.012>.
- (18) Vuitton, V.; Yelle, R. V.; Klippenstein, S. J.; Hörst, S. M.; Lavvas, P. Simulating the Density of Organic Species in the Atmosphere of Titan with a Coupled Ion-Neutral Photochemical Model. *Icarus* **2019**, *324*, 120–197. <https://doi.org/10.1016/j.icarus.2018.06.013>.
- (19) Cui, J.; Yelle, R. V.; Vuitton, V.; Waite, J. H.; Kasprzak, W. T.; Gell, D. A.; Niemann, H. B.; Müller-Wodarg, I. C. F.; Borggren, N.; Fletcher, G. G.; et al. Analysis of Titan's Neutral Upper Atmosphere from Cassini Ion Neutral Mass Spectrometer Measurements. *Icarus* **2009**, *200* (2), 581–615. <https://doi.org/10.1016/j.icarus.2008.12.005>.
- (20) Balucani, N.; Skouteris, D.; Leonori, F.; Petrucci, R.; Hamberg, M.; Geppert, W. D.; Casavecchia, P.; Rosi, M. Combined Crossed Beam and Theoretical Studies of the N(2D) + C<sub>2</sub>H<sub>4</sub> Reaction and Implications for Atmospheric Models of Titan. *J. Phys. Chem. A* **2012**, *116* (43), 10467–10479. <https://doi.org/10.1021/jp3072316>.
- (21) Balucani, N.; Skouteris, D. Gas-Phase Prebiotic Chemistry Driven by Ultraviolet Photolysis of Simple Molecules. In *Prebiotic Photochemistry: From Urey–Miller-like Experiments to Recent Findings*; Saija, F., Cassone, G., Eds.; The Royal Society of Chemistry, 2021; pp 37–59. <https://doi.org/10.1039/9781839161773-00037>.
- (22) He, C.; Serigano, J.; Hörst, S. M.; Radke, M.; Sebree, J. A. Titan Atmospheric Chemistry Revealed by Low-Temperature N<sub>2</sub>-CH<sub>4</sub> Plasma Discharge Experiments. *ACS Earth Sp. Chem.* **2022**, *6* (10), 2295–2304. <https://doi.org/10.1021/acsearthspacechem.2c00164>.
- (23) Brown, R.; Winkler, C. A. The Chemical Behavior of Active Nitrogen. *Angew. Chemie Int. Ed. English* **1970**, *9* (3), 181–196. <https://doi.org/10.1002/anie.197001811>.
- (24) Herron, J. T. Evaluated Chemical Kinetics Data for Reactions of N(2D), N(2P), and N<sub>2</sub>(A<sup>3</sup>Σ<sup>+</sup>) in the Gas Phase. *J. Phys. Chem. Ref. Data* **1999**, *28*, 1453–1483. <https://doi.org/10.1002/9780470145296.ch116>.
- (25) Suzuki, T.; Shihira, Y.; Sato, T.; Umemoto, H.; Tsunashima, S. Reactions of N(2D) and N(2P) with H<sub>2</sub> and D<sub>2</sub>. *J. Chem. Soc. Faraday Trans.* **1994**, *89*, 995–999. <https://doi.org/10.1039/FT9938900995>.
- (26) Donovan, R. J.; Husain, D. Recent Advances in the Chemistry of Electronically

- Excited Atoms. *Chem. Rev.* **1970**, *70* (4), 489–516.  
<https://doi.org/10.1021/cr60266a003>.
- (27) Schofield, K. Critically Evaluated Rate Constants for Gaseous Reactions of Several Electronically Excited Species. *J. Phys. Chem. Ref. Data* **1979**, *8*, 723–798.  
<https://doi.org/10.1063/1.555606>.
- (28) Vanuzzo, G.; Marchione, D.; Mancini, L.; Liang, P.; Pannacci, G.; Recio, P.; Tan, Y.; Rosi, M.; Skouteris, D.; Casavecchia, P.; et al. The N(2D) + CH<sub>2</sub>CHCN (Vinyl Cyanide) Reaction: A Combined Crossed Molecular Beam and Theoretical Study and Implications for the Atmosphere of Titan. *J. Phys. Chem. A* **2022**, *126* (36), 6110–6123. <https://doi.org/10.1021/acs.jpca.2c04263>.
- (29) Mancini, L.; Vanuzzo, G.; Marchione, D.; Pannacci, G.; Liang, P.; Recio, P.; Rosi, M.; Skouteris, D.; Casavecchia, P.; Balucani, N. The Reaction N(2D) + CH<sub>3</sub>CCH (Methylacetylene): A Combined Crossed Molecular Beams and Theoretical Investigation and Implications for the Atmosphere of Titan. *J. Phys. Chem. A* **2021**, *125* (40), 8846–8859. <https://doi.org/10.1021/acs.jpca.1c06537>.
- (30) Recio, P.; Marchione, D.; Caracciolo, A.; Murray, V. J.; Mancini, L.; Rosi, M.; Casavecchia, P.; Balucani, N. A Crossed Molecular Beam Investigation of the N(2D) + Pyridine Reaction and Implications for Prebiotic Chemistry. *Chem. Phys. Lett.* **2021**, *779* (March), 138852. <https://doi.org/10.1016/j.cplett.2021.138852>.
- (31) Hickson, K. M.; Bray, C.; Loison, J. C.; Dobrijevic, M. A Kinetic Study of the N(2D) + C<sub>2</sub>H<sub>4</sub> reaction at Low Temperature. *Phys. Chem. Chem. Phys.* **2020**, *22* (25), 14026–14035. <https://doi.org/10.1039/d0cp02083d>.
- (32) Geiger, J.; Schröder, B. Intensity Perturbations Due to Configuration Interaction Observed in the Electron Energy-Loss Spectrum of N<sub>2</sub>. *J. Chem. Phys.* **1969**, *50* (1), 107–119. <https://doi.org/10.1063/1.1670870>.
- (33) Liu, M.; Jiang, P.; Cheng, M.; Gao, H. Vacuum Ultraviolet Photoexcitation and Photofragment Spectroscopic Studies of <sup>14</sup>N<sup>15</sup>N between 109000 and 117500 Cm<sup>-1</sup>. *J. Chem. Phys.* **2021**, *155* (23), 234305. <https://doi.org/10.1063/5.0072604>.
- (34) Spelsberg, D.; Meyer, W. Dipole-Allowed Excited States of N<sub>2</sub>: Potential Energy Curves, Vibrational Analysis, and Absorption Intensities. *J. Chem. Phys.* **2001**, *115* (14), 6438–6449. <https://doi.org/10.1063/1.1400139>.
- (35) Zipf, E. C.; McLaughlin, R. W. On the Dissociation of Nitrogen by Electron Impact and by EUV Photo-Absorption. *Planet. Sp. Sci.* **1977**, *26*, 449–462.  
<https://doi.org/10.1103/PhysRev.34.743>.

- (36) Helm, H.; Cosby, P. C. Product Branching in Predissociation of the  $e\ 1\Pi_u$ ,  $E'1\Sigma_u^+$ , and  $B' 1\Sigma_u^+$  States of  $N_2$ . *J. Chem. Phys.* **1989**, *90* (8), 4208–4215. <https://doi.org/10.1063/1.455777>.
- (37) Walter, C. W.; Cosby, P. C.; Helm, H.  $N(4S_0)$ ,  $N(2D_0)$ , and  $N(2P_0)$  Yields in Predissociation of Excited Singlet States of  $N_2$ . *J. Chem. Phys.* **1993**, *99* (5), 3553–3561.
- (38) Walter, C. W.; Cosby, P. C.; Helm, H. Predissociation Quantum Yields of Singlet Nitrogen. *Phys. Rev. A* **1994**, *50* (4), 2930–2936.
- (39) Chakraborty, S.; Muskatel, B. H.; Jackson, T. L.; Ahmed, M.; Levine, R. D.; Thiemens, M. H.; Cerling, T. E. Massive Isotopic Effect in Vacuum UV Photodissociation of  $N_2$  and Implications for Meteorite Data. *Proc. Natl. Acad. Sci. U. S. A.* **2014**, *111* (41), 14704–14709. <https://doi.org/10.1073/pnas.1410440111>.
- (40) Chakraborty, S.; Jackson, T. L.; Rude, B.; Ahmed, M.; Thiemens, M. H. Nitrogen Isotopic Fractionations in the Low Temperature (80 K) Vacuum Ultraviolet Photodissociation of  $N_2$ . *J. Chem. Phys.* **2016**, *145* (11), 114302. <https://doi.org/10.1063/1.4962447>.
- (41) Song, Y.; Gao, H.; Chang, Y. C.; Hammoutène, D.; Ndome, H.; Hochlaf, M.; Jackson, W. M.; Ng, C. Y. Quantum-State Dependence of Product Branching Ratios in Vacuum Ultraviolet Photodissociation of  $N_2$ . *Astrophys. J.* **2016**, *819*, 23. <https://doi.org/10.3847/0004-637x/819/1/23>.
- (42) Liu, M.; Jiang, P.; Lu, L.; Yin, T.; Ma, L.; Cheng, M.; Yin, Q.; Gao, H. Strong Isotope-Dependent Photodissociation Branching Ratios of  $N_2$  and Their Potential Implications for the  $^{14}N/^{15}N$  Isotope Fractionation in Titan's Atmosphere. *Astrophys. J.* **2021**, *923* (2), 196. <https://doi.org/10.3847/1538-4357/ac2f97>.
- (43) Jiang, P.; Lu, L.; Liu, M.; Gao, H. Multi-Channel Photodissociation Dynamics of  $^{14}N_2$  in Its  $B' 1\Sigma^+u(v = 20)$  State. *Phys. Chem. Chem. Phys.* **2022**, *24* (19), 11544–11551. <https://doi.org/10.1039/d2cp01148d>.
- (44) Lu, L.; Jiang, P.; Gao, H. Accurate Measurements of the Bond Dissociation Energies of  $^{14}N_2$ ,  $^{14}N^{15}N$  and  $^{15}N_2$ . *Fundam. Res.* **2022**. <https://doi.org/10.1016/j.fmre.2022.08.003>.
- (45) Sharpe, S. W.; Johnson, P. M. Triplet Rydberg States in Molecular Nitrogen. *J. Chem. Phys.* **1986**, *85* (9), 4943–4948. <https://doi.org/10.1063/1.451732>.
- (46) Lewis, B. R.; Heays, A. N.; Gibson, S. T.; Lefebvre-Brion, H.; Lefebvre, R. A. Coupled-Channel Model of the  $3\Pi_u$  States of  $N_2$ : Structure and Interactions of the

- 3s $\sigma$ gF 3 3 $\Pi$ u and 3p $\pi$ uG3 3 $\Pi$ u Rydberg States. *J. Chem. Phys.* **2008**, *129*, 164306. <https://doi.org/10.1063/1.2990656>.
- (47) Minaev, B.; Norman, P.; Jonsson, D.; Ågren, H. Response Theory Calculations of Singlet-Triplet Transitions in Molecular Nitrogen. *Chem. Phys.* **1995**, *190* (1), 11–29. [https://doi.org/10.1016/0301-0104\(94\)00321-Z](https://doi.org/10.1016/0301-0104(94)00321-Z).
- (48) Qin, Z.; Zhao, J.; Liu, L. Radiative Transition Probabilities between Low-Lying Electronic States of N<sub>2</sub>. *Mol. Phys.* **2019**, *117* (18), 2418–2433. <https://doi.org/10.1080/00268976.2018.1562579>.
- (49) Minaev, B. F.; Panchenko, O. O.; Minaeva, V. A.; Ågren, H. Triplet State Harvesting and Search for Forbidden Transition Intensity in the Nitrogen Molecule. *Front. Chem.* **2022**, *10* (October), 1–10. <https://doi.org/10.3389/fchem.2022.1005684>.
- (50) Minaev, B.; Da Silva, R. S.; Panchenko, O.; Ågren, H. Prediction of New Spin-Forbidden Transitions in the N<sub>2</sub> Molecule - The Electric Dipole A'<sup>5</sup>Σ<sub>g</sub><sup>+</sup>→ A<sub>3</sub>Σ<sub>u</sub><sup>+</sup> and Magnetic Dipole A'<sup>1</sup>Σ<sub>u</sub><sup>-</sup>← A<sub>3</sub>Σ<sub>u</sub><sup>+</sup> Transitions. *J. Chem. Phys.* **2023**, *158* (8), 084304. <https://doi.org/10.1063/5.0136465>.
- (51) Gilmore, F. R. Potential Energy Curves for N<sub>2</sub>, NO, O<sub>2</sub> and Corresponding Ions. *J. Quant. Spectrosc. Radiat. Transf.* **1965**, *5* (2), 369–389. [https://doi.org/10.1016/0022-4073\(65\)90072-5](https://doi.org/10.1016/0022-4073(65)90072-5).
- (52) Lefebvre-Besson, H.; Moser, C. M. Calculation of Rydberg Levels in the Nitrogen Molecule. *J. Chem. Phys.* **1965**, *43* (4), 1394–1399. <https://doi.org/10.1063/1.1696931>.
- (53) Little, D. A.; Tennyson, J. An Ab Initio Study of Singlet and Triplet Rydberg States of N<sub>2</sub>. *J. Phys. B At. Mol. Opt. Phys.* **2013**, *46* (14), 145102. <https://doi.org/10.1088/0953-4075/46/14/145102>.
- (54) Ermler, W. C.; Clark, J. P.; Mulliken, R. S. Ab Initio Calculations of Potential Energy Curves and Transition Moments of 1Σ<sub>g</sub><sup>+</sup> and 1Σ<sub>u</sub><sup>+</sup> States of N<sub>2</sub>. *J. Chem. Phys.* **1987**, *86* (1), 370–375. <https://doi.org/10.1063/1.452573>.
- (55) Hochlaf, M.; Ndome, H.; Hammoutne, D. Quintet Electronic States of N<sub>2</sub>. *J. Chem. Phys.* **2010**, *132* (10), 104310. <https://doi.org/10.1063/1.3359000>.
- (56) Hochlaf, M.; Ndome, H.; Hammoutène, D.; Vervloet, M. Valence-Rydberg Electronic States of N<sub>2</sub>: Spectroscopy and Spin-Orbit Couplings. *J. Phys. B At. Mol. Opt. Phys.* **2010**, *43* (24), 245101. <https://doi.org/10.1088/0953-4075/43/24/245101>.
- (57) Adamson, S. O.; Kuverova, V. V.; Ozerov, G. K.; Golubkov, G. V.; Nabiev, S. S.; Golubkov, M. G. Ab Initio Calculation of the Lowest Singlet and Triplet Excited States of the N<sub>2</sub> Molecule. *Russ. J. Phys. Chem. B* **2018**, *12* (4), 620–631.

- <https://doi.org/10.1134/S1990793118040024>.
- (58) Bhattacharya, D.; Shamasundar, K. R.; Emmanouilidou, A. Potential Energy Curves of Molecular Nitrogen for Singly and Doubly Ionized States with Core and Valence Holes. *J. Phys. Chem. A* **2021**, *125* (36), 7778–7787.  
<https://doi.org/10.1021/acs.jpca.1c04613>.
- (59) Stahel, D.; Leoni, M.; Dressler, K. Nonadiabatic Representations of the  $1\Sigma^+$  and  $1\Pi_u$  States of the N<sub>2</sub> Molecule. *J. Chem. Phys.* **1983**, *79* (6), 2541–2558.  
<https://doi.org/10.1063/1.446166>.
- (60) Curchod, B. F. E.; Martínez, T. J. Ab Initio Nonadiabatic Quantum Molecular Dynamics. *Chemical Reviews*. 2018, pp 3305–3336.  
<https://doi.org/10.1021/acs.chemrev.7b00423>.
- (61) Schlegel, H. B. Ab Initio Direct Dynamics. *Acc. Chem. Res.* **2021**, *54* (20), 3749–3759. <https://doi.org/10.1021/acs.accounts.1c00390>.
- (62) Nisoli, M.; Decleva, P.; Calegari, F.; Palacios, A.; Martín, F. Attosecond Electron Dynamics in Molecules. *Chem. Rev.* **2017**, *117* (16), 10760–10825.  
<https://doi.org/10.1021/acs.chemrev.6b00453>.
- (63) Lassmann, Y.; Hollas, D.; Curchod, B. F. E. Extending the Applicability of the Multiple-Spawning Framework for Nonadiabatic Molecular Dynamics. *J. Phys. Chem. Lett.* **2022**, *13*, 12011–12018. <https://doi.org/10.1021/acs.jpcclett.2c03295>.
- (64) Gelfand, N.; Komarova, K.; Remacle, F.; Levine, R. D. Nonadiabatic Dynamics in a Forest of Coupled States: Electronic State Branching in the VUV Photodissociation of N<sub>2</sub>. *J. Chem. Phys.* **2023**, *158*, 164302. <https://doi.org/10.1063/5.0148798>.
- (65) Lefebvre-Brion, H.; Field, R. W. *The Spectra and Dynamics of Diatomic Molecules*; Elsevier: Amsterdam, 2004.
- (66) Werner, H. J.; Knowles, P. J. A Second Order Multiconfiguration SCF Procedure with Optimum Convergence. *J. Chem. Phys.* **1985**, *82* (11), 5053–5063.  
<https://doi.org/10.1063/1.448627>.
- (67) Knowles, P. J.; Werner, H. J. An Efficient Second-Order MC SCF Method for Long Configuration Expansions. *Chem. Phys. Lett.* **1985**, *115* (3), 259–267.  
[https://doi.org/10.1016/0009-2614\(85\)80025-7](https://doi.org/10.1016/0009-2614(85)80025-7).
- (68) Werner, H. J.; Knowles, P. J.; Knizia, G.; Manby, F. R.; Schütz, M. Molpro: A General-Purpose Quantum Chemistry Program Package. *Wiley Interdiscip. Rev. Comput. Mol. Sci.* **2012**, *2* (2), 242–253. <https://doi.org/10.1002/wcms.82>.
- (69) Werner, H. J.; Knowles, P. J.; Manby, F. R.; Black, J. A.; Doll, K.; Heßelmann, A.;

- Kats, D.; Köhn, A.; Korona, T.; Kreplin, D. A.; et al. The Molpro Quantum Chemistry Package. *J. Chem. Phys.* **2020**, *152*, 144107. <https://doi.org/10.1063/5.0005081>.
- (70) Ajay, J. S.; Komarova, K. G.; Wildenberg, S. Van Den; Remacle, F.; Levine, R. D. Attophotochemistry: Coherent Electronic Dynamics and Nuclear Motion. In *Theoretical and Computational Chemistry Series*; Vrakking, M. J. J., Lepine, F., Eds.; The Royal Society of Chemistry: Cambridge, 2018; pp 308–347.
- (71) Li, X.; Heays, A. N.; Visser, R.; Ubachs, W.; Lewis, B. R.; Gibson, S. T.; Van Dishoeck, E. F. Photodissociation of Interstellar N<sub>2</sub>. *Astron. Astrophys.* **2013**, *555*, A14. <https://doi.org/10.1051/0004-6361/201220625>.